Materials Research Bulletin 48 (2013) 1040–1044

Contents lists available at SciVerse ScienceDirect

Materials Research Bulletin

journal homepage: www.elsevier.com/locate/matresbu

Controllable synthesis, growth mechanism and optical properties of the ZnSe quantum dots and nanoparticles with different crystalline phases

Bo Feng [a,b,c], Jinghai Yang [c,*], Jian Cao [c], Lili Yang [c], Ming Gao [c], Maobin Wei [c], Yang Liu [c], Hang Song [a]

[a] Key Laboratory of Excited State Physics, Changchun Institute of Optics, Fine Mechanics and Physics, Chinese Academy of Sciences, 3888 Eastern Nan-Hu Road, Changchun 130033, PR China
[b] Graduate School of the Chinese Academy of Sciences, Beijing 100049, PR China
[c] Institute of Condensed State Physics, Jilin Normal University, Siping 136000, PR China

ARTICLE INFO

Article history:
Received 7 June 2012
Received in revised form 8 October 2012
Accepted 25 November 2012
Available online 3 December 2012

Keywords:
A. Nanostructures
A. Semiconductors
B. Chemical synthesis
D. Optical properties

ABSTRACT

ZnSe precursors were prepared by a solvothermal method at 180 °C without any surface-active agents. ZnSe quantum dots and nanoparticles were obtained by annealing the precursors at 300 °C for 2 h in argon atmosphere. The ZnSe quantum dots were about 3.5 nm, while the ZnSe nanoparticles were about 21 nm, as observed using TEM. The growth mechanisms for the two samples were discussed; this proved that the high coordination ability of ethylenediamine to zinc played an important role in the final phase of the products. The ZnSe quantum dots with the wurtzite structure exhibited a strong near band-edge emission (NBE) peak centered at 422 nm, which was blue-shifted in comparison to that of the bulk ZnSe, which was mainly caused by the quantum confinement effect. However, the zinc blende ZnSe nanoparticles exhibited a near-band-edge luminescence peak centered at 472 nm.

1. Introduction

The preparation and characterization of nanostructured materials with a defined size and morphology have attracted much attention recently due to their great potential for fundamental research and practical applications in the fields of electroluminescent materials, solar cells, sensors, and optical recording materials [1–4]. Zinc selenide is an important II–VI semiconductor that is extremely important for applications, such as laser diodes, light-emitting diodes, and photodetectors, due to its wide band gap and large exciton binding energy (21 meV) [5–8]. ZnSe has two stable phase structures: the cubic zinc blende (ZB) at low temperatures and the hexagonal wurtzite (WZ) at high temperatures [9–11]. The WZ ZnSe structure is thermodynamically metastable at the low temperatures in general and its formation requires extreme conditions. Due to the high-reaction temperature it is probable that different phases coexist. Due to the slight structural differences between the ZB and WZ structures, subtle differences of synthetic conditions can favor one polymorph over the other. Consequently, it is still a challenge to predictably generate WZ polymorphs and understand the types of factors that play a key role in their formation.

High-quality colloidal semiconductor nanocrystals (also referred to quantum dots, QDs) have found useful applications in a wide range of fields from biology to materials science. Their unique properties, such as tuning emission wavelengths, can be observed due to quantum confinement effects caused by their small size. ZnSe QDs are excellent UV-blue emitters and considered to be the leading candidate for the fabrication of blue LEDs and LDs [12,13]. Furthermore, due to their low toxicity (without heavy metal ions), ZnSe QDs are potential blue fluorescent biological labels. Therefore, many attempts have been made to develop methods for the synthesis of ZnSe QDs and nanoparticles (NPs) due to their size-dependent properties and potential applications in various fields. For example, Hines and Guyot-Sionnest first reported that high luminescent ZnSe was prepared with organometallic diethylzinc in a trioctylphosphine oxide (TOPO)-hexadecylamine (HAD) mixture [14]. ZnSe QDs prepared by this method had a high quantum yield (QY) of up to 20–50%, as well as high crystallinity and monodispersity. Panda et al. synthesized shape-, size-, and phase-controlled ZnSe NPs and nanorods using liganding solvents of octadecylamine (ODA) and trioctylphosphine oxide (TOPO) [15–17]. However, these methods usually involve sophisticated equipment, expensive organic additives, or toxic reagents, which are not environmentally friendly, and require rigorous conditions in order to protect the reaction reagents from oxidation. Accordingly, there is an urgent need to develop a simple and non-toxic method to synthesize ZnSe QDs.

* Corresponding author.
E-mail address: jhyang1@jlnu.edu.cn (J. Yang).

0025-5408/$ – see front matter © 2012 Elsevier Ltd. All rights reserved.
http://dx.doi.org/10.1016/j.materresbull.2012.11.100

In this paper, we synthesize ZnSe QDs with WZ structure and NPs with ZB structure, using the solvothermal method and different solvents (EN or EDTA). This method requires a relatively low temperature and cheap precursors that have low toxicity; also it is simple and easy to perform. Although different nanomaterials have been synthesized using EDTA or EN, reports about the growth mechanism are rare. Also a literature search has shown that there is no previous work comparing the PL properties of ZnSe samples with different sizes and crystalline phases. Thus, we will compare the distinguishable size- and structure- dependent optical properties of ZnSe nanomaterials and investigate in detail the growth mechanism of ZnSe nanostructures obtained using different solvents.

2. Experimental

All chemicals were of analytical grade and used as received, without further purification.

The synthesis of the ZnSe precursors was carried out using the following procedures: $Zn(NO_3)_2{\cdot}6H_2O$ (0.5 mmol) was dissolved in 30 ml water and selenium powder (99.95%) (0.5 mmol) in 30 ml of ethylenediamine (EN). $Zn(NO_3)_2{\cdot}6H_2O$ (0.5 mmol) was dissolved in 30 ml of EDTA solution and selenium powder (99.95%) (0.5 mmol) in 30 ml of NaOH solution. After stirring for 1 h, water and EN were added into one beaker, while EDTA solution and NaOH solution into anther beaker. Then after stirring for a further hour, the mixed solution was transferred into two 80-ml Teflon-lined autoclaves. The autoclaves were sealed and heated at 180 °C for 30 h. When the reaction was complete the autoclaves were cooled to the room temperature. The products were washed with ethanol and deionized water several times and then separated by centrifugation. They were then dried at 60 °C for 1 h to obtain the precursors. Finally, the precursors were annealed at 300 °C for 2 h to produce the samples.

2.1. Characterization

The X-ray diffraction (XRD) pattern was collected on a MAC Science MXP-18 X-ray diffractometer using a Cu target radiation source. A transmission electron micrograph (TEM) was taken with a JEM-2100 electron microscope. The specimen was prepared by depositing a drop of the dilute sample solution in 2-propanol on a carbon-coated copper grid and drying at room temperature. An energy dispersive X-ray analysis (EDAX) system attached to the SEM was employed to analyze the chemical composition. PL measurement was carried out at room temperature, using 325 nm as the excitation wavelength, and a He–Cd laser as the excitation source. The Raman scattering studies were performed with a 1000B Renishaw micro-Raman system in the back-scattering configuration, and the excitation source was the 514.5 nm line of an Ar^+ laser for which ZnSe was transparent. The beam was focused through a microscope objective on the samples as a 1 μm circular spot.

3. Results and discussion

The XRD patterns of the ZnSe QDs and NPs are shown in Fig. 1. For the QDs in Fig. 1(a), all the diffraction peaks can be well indexed as being in the hexagonal wurtzite phase, which is consistent with the standard card (P63mc, JCPDS No. 80-0008). No other diffraction peaks can be identified in the pattern, indicating no impurities exist in the as-grown sample. For the NPs in Fig. 1(b), the peaks centered at 27.20°, 45.17°, 53.53°, 65.82° and 72.59 ° closely match the (1 1 1), (2 2 0), (3 1 1), (4 0 0) and (3 3 1) diffraction planes of the cubic zinc blende ZnSe ($F\bar{4}3$ m, JCPDS file 37-1463). As the QDs have a small size the diffraction peaks are considerably broader from the QDs than the NPs.

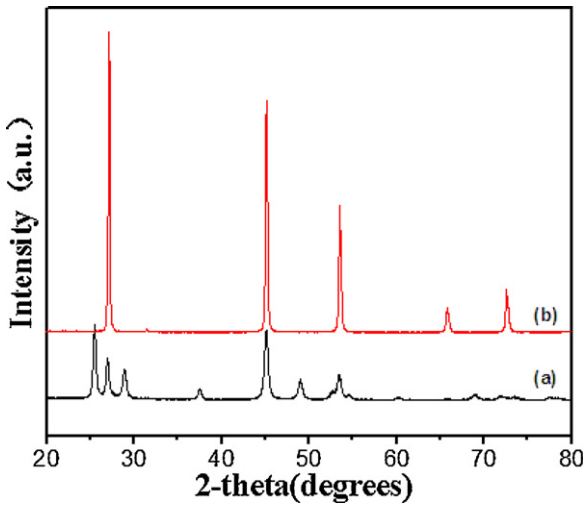

Fig. 1. XRD patterns of ZnSe QDs (a) and NPs (b).

Moreover, the lattice constant 'a' and 'c' for the hexagonal structure and 'a' for the cubic structure can be determined from the relationships:

$$\text{Hexagonal}: \quad \frac{1}{d_{hkl}^2} = \frac{4}{3}\left\{\frac{h^2+hk+k^2}{a^2}\right\} + \frac{l^2}{c^2}$$

$$\text{Cubic}: \quad \frac{1}{d_{hkl}^2} = \frac{h^2+k^2+l^2}{a^2}$$

The average lattice constants of 'a' and 'c' for QDs are found to be $a = 3.999$ Å, $c = 6.568$ Å and the corresponding $c/a = 1.6426$, which is slightly larger than the standard value of 1.6371. The average lattice constant of 'a' for NPs is found to be 5.673 Å, which is also slightly larger than the standard value of 5.668 Å. These results indicate that both the QDs and the NPs are under tensile strain.

Fig. 2 presents the TEM micrograph of the ZnSe QDs with WZ structure and the ZnSe NPs with ZB structure. The average QDs size is about 3–4 nm in Fig. 2(a) and (b), with a spherical shape and narrow size distribution. The HRTEM images of the QDs (the insets in Fig. 2(b)) show that the interplanner separations (d) are about 0.34 nm along the (1 0 0) plane of the ZnSe, which is consistent with the WZ structure of ZnSe. Fig. 2(c) is the TEM image of the ZnSe NPs, which shows that the size of the NPs is about 21 nm. The HRTEM image of ZnSe NPs (Fig. 2(d)) shows the well-defined lattice planes, which reflect a high degree of crystallinity within each individual crystal. The interplanar distance of 0.33 nm is consistent with the ZB structure of ZnSe. The EDAX analysis in Fig. 2(e) and (f) of the ZnSe QDs with WZ structure and NPs with ZB structure indicates that both samples are composed of Zn and Se elements (other peaks arise from Au) and the Zn:Se atomic ratio is approximately 1:1.

The role of EN in the formation of the ZnSe precursors can be explained by the solvent coordination molecular template (SCMT) mechanism [18]. Taking the thermodynamic aspects into consideration, during the process of heating the ZnSe precursors under an inert atmosphere, the EN must be lost. Another important factor for finally inducing the formation of ZnSe NPs is the kinetics of the SCMT process. The possible growth mechanism can be described as follows:

$$Se + NH_2CH_2CH_2NH_2 \rightarrow Se^{2-}$$

$$ZnSe \cdot EN_{0.5} \rightarrow ZnSe \downarrow + 0.5EN.$$

We find that the EDTA plays a key role in the formation of the ZnSe NPs. EDTA is a complex one with a polyfunctional group in the form of 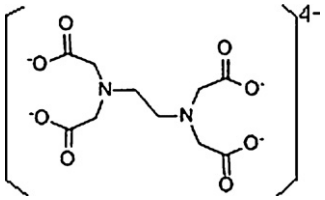 in aqueous solution. The hydrophilic carboxyls act as the templates for the micelle structure [19]. So EDTA acts as both the bridge complexing agent and micelle

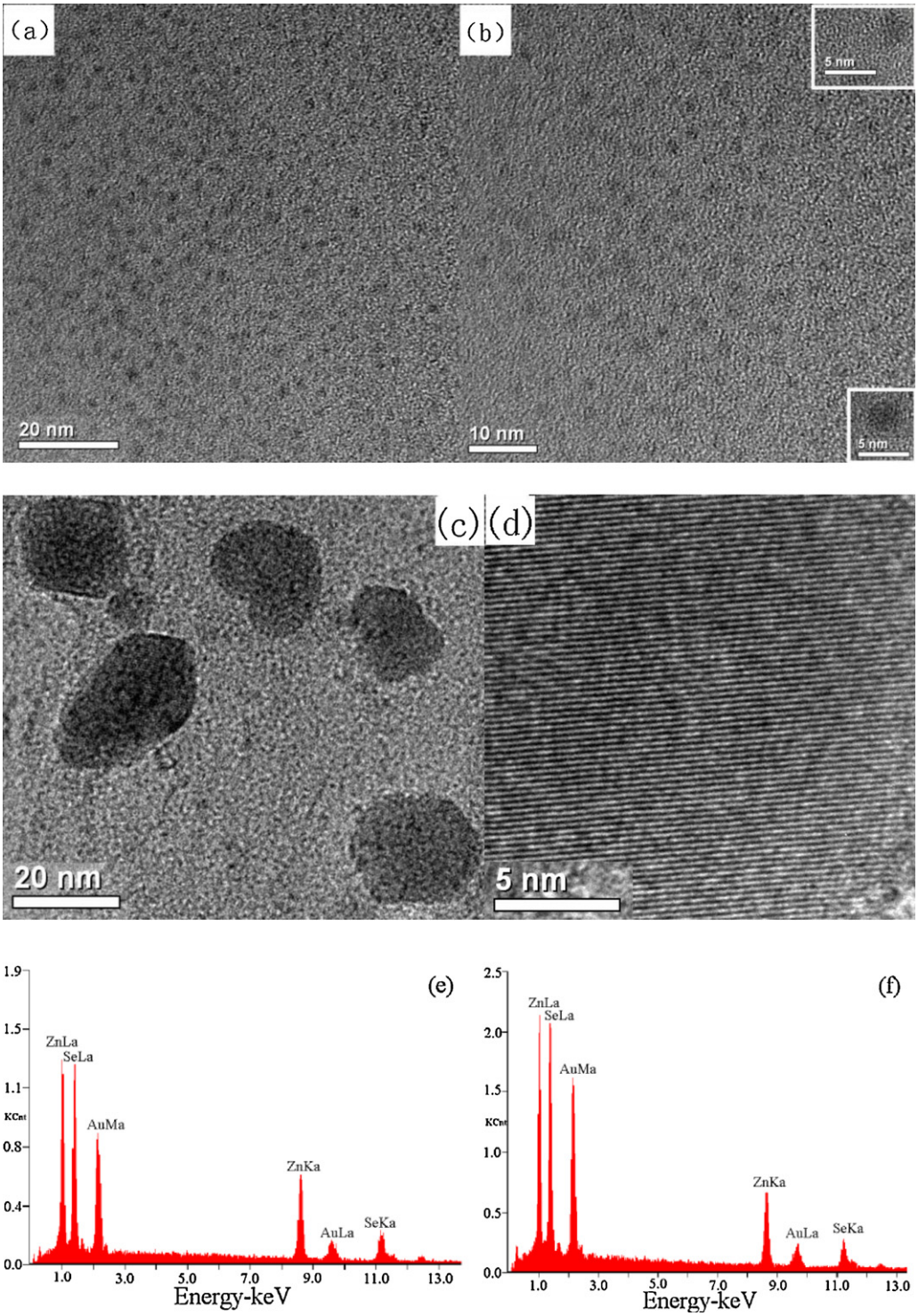

Fig. 2. TEM images of ZnSe QDs with wurtzite structure (a); (b) the insets in (b) are high-resolution TEM images; (c) TEM images of ZnSe NPs with cubic structure; (d) high-resolution TEM images of ZnSe NPs; (e) EDAX spectrum of ZnSe QDs with wurtzite structure; (f) EDAX spectrum of ZnSe NPs with cubic structure.

like soft-template, which finally forms the coordination compound with Zn^{2+} in the growth process of ZnSe NPs. Then Se^{2-} reacts with the coordination compound and forms the ZnSe NPs.

The possible growth mechanism can be described as follows:

$$3Se + 6OH^- \rightarrow 2Se^{2-} + SeO_3{}^{2-} + 3H_2O$$

$$Zn(NO_3)_2 + EDTA \rightarrow [Zn(EDTA)]^{2+} + 2NO_3{}^-$$

$$[Zn(EDTA)]^{2+} \rightarrow Zn^{2+} + EDTA$$

$$Se^{2-} + Zn^{2+} \rightarrow ZnSe$$

It is common knowledge that ZnSe has two polymorphs: the cubic sphalerite and the hexagonal wurtzite. Differences in the two structures are to do with the order in which the closed planes are stacked. A stacking of ABAB forms the hexagonal wurtzite, while that of ABCABC forms the cubic sphalerite. As EN has high coordination ability to zinc ($\log \beta[Zn(en)_2]^{2+} = 10.83$) it makes EN interrelated zinc chalcogenides attractive. So, it can be concluded that the complexing ability of groups containing atom N can effectively determine the final phase of the products. The WZ ZnSe crystal is described as alternating the stacking of positively charged Zn and negatively charged Se ions along its *c* axis. The WZ structure, which ensures the anisotropy characteristic, is preferred due to the template effect of EN. The results reveal that EN, as a solvent, favors the formation of wurtzite ZnSe nanostructure [7].

The optical properties of the ZnSe QDs and NPs are examined by PL spectroscopy. Fig. 3 displays the room-temperature PL emission spectra of the ZnSe QDs with WZ structure and NPs with ZB structure. For QDs with WZ structure, in Fig. 3(a), the PL spectrum comprises two emission bands—a strong emission band centered at 422 nm and a weak defect-related emission band extending from 550 to 585 nm. The emission band around 422 nm is usually attributed to the near band-edge (NBE) emission of ZnSe [12]. In this case, the peak position exhibits an obvious blue-shifted phenomenon, when compared with the PL spectra of bulk WZ ZnSe. Since the QDs have a particle radius significantly smaller than the exciton Bohr radius, they show strong size-dependent optical properties due to the quantum confinement effect. Cooper et al. studied the PL spectrum of ZnSe QDs and found a major emission band peak at 427 nm, which was a similar result to that presented here. Chen et al. synthesized colloidal ZnSe QDs from ZnO powder successfully, and the QDs showed controlled PL emission from 400 to 440 nm [12]. A strong main emission band found at 436 nm has been reported by Panda et al. in the PL spectrum of the ZnSe nanostructures [15]. Our results (422 nm) have a greater blue-shifted than theirs, indicating a smaller size for the synthesized sample.

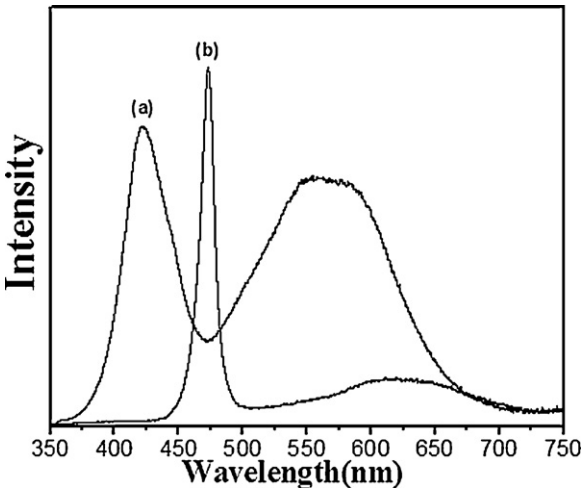

Fig. 3. Room-temperature PL (excited at 325 nm) of ZnSe QDs (a) and NPs (b).

For NPs with ZB structure, in Fig. 3(b), the spectrum exhibits a strong and stable blue emission peak at 472 nm. The room temperature PL peak position is not always consistent, for example, transition energy from 466 nm [20] to 476 nm [21]. The exact energy position depends on the contribution between the FX, FX-phonon replica, and the transition of free electrons to acceptor bound holes. A weak emission band ranging from 600 to 640 nm is also identified. The strong blue emission peak is usually attributed to the NBE emission of ZnSe, which is associated with the free excitons, while the broad peak is a defect-related emission. Compared with ZnSe NPs grown by others [22,23], the NPs synthesized here show significantly higher intensity in the NBE peak, relative to the defect-related emission peak, which indicates their better optical properties. The strong band-edge luminescence is connected with a low density of dislocations, as well as a low density of surface defects, as these defects tend to quench the band-edge radiative recombination. The weakness of the deep-level emissions also suggests that these NPs are of stoichiometric composition, with perhaps a low density of point defects. These results are in agreement with those of XRD and TEM.

For NPs with ZB structure, the diameters are larger than the Bohr exciton diameter of ZnSe, so, the optical behavior of the NPs should be similar to that of the bulk. Generally, the intensity ratio of the NBE emission band to the defect-related emission band is regarded as an indicator of the crystallinity of semiconductor materials. The larger the intensity ratio the better the materials crystallization will be. The relative PL intensity ratio of NBE emission (I_{NBE}) to defect-related emission (I_{DRE}) of QDs with WZ structure and NPs with ZB structure is estimated to be about 0.511 and 3.649, respectively. It can be seen that the NPs with ZB structure have much better crystallization according to the larger intensity ratio. This difference in relative intensities can be accounted for by the smaller size and higher surface-to-volume ratio in QDs than in NPs. Moreover, the NPs have a lower surface energy than the QDs, and a lower density of surface defects, consequently their defect-related emissions becomes lower. The larger ZnSe NPs have a continuous surface with localized trapping defects related to the core lattice, while the smaller ZnSe QDs are found to have a discontinuous surface. Therefore, the valence and conduction bands are replaced by more widely spaced individual energy levels in the smaller sizes, the lowest of which gives rise to the observed luminescence [24]. The above results further support the results obtained from XRD and TEM.

Raman scattering is very sensitive to the microstructure of nano-sized materials. Fig. 4 shows a typical room-temperature Raman spectrum of ZnSe QDs and NPs. As seen from Fig. 4(a) for as-synthesized ZnSe QDs with WZ structure, two Raman peaks centered at 205 and 251 cm^{-1} are observed, which are attributed to the transverse optic (TO) and longitudinal optic (LO) phonon modes of crystalline ZnSe, respectively. The positions of the LO modes shift from 255 (bulk ZnSe values) to 253 cm^{-1}, and the LO phonon frequency exhibit a broad Raman peak due to the high surface to volume ratio of small particles. Large homogeneous broadening of Raman spectra seems to be a common characteristic of nanomaterials with small diameters in the II–VI group [25,26]. As nanocrystals have small dimensions the mean free path of phonons is reduced and therefore they frequently collide and relax

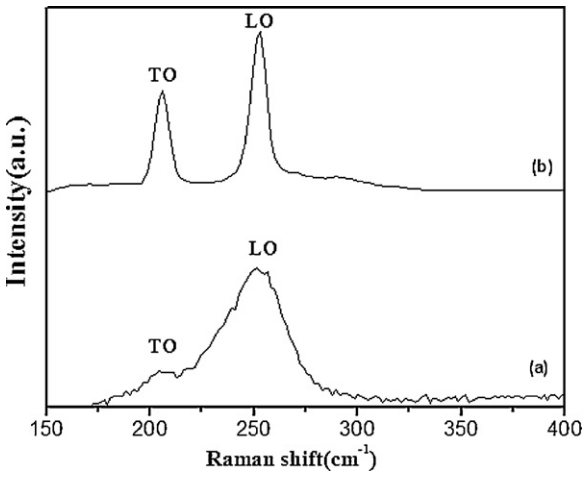

Fig. 4. Raman spectrum of ZnSe QDs (a) and NPs (b), 514.5 nm excitation.

at the interface. Lattice distortion and structure defects are common features of most nanostructured materials, which also results in a shortening of the lifetime of phonons and contributes to the large homogeneous broadening [26]. From the theoretical point of view, some surface modes should be Raman active. For bulk material, the surface modes are very few compared to the bulk modes, and they cannot be observed. But for small nanocrystals, especially when the ionic microcrystal size is smaller than the wavelength of the incident light in the crystal, surface modes can be observed. It is believed that the surface phonon modes are responsible for the asymmetry in the lower frequency part of the ZnSe QDs Raman scattering. The appearance of surface phonons is a characteristic feature of small-size nanostructures [25,27,28].

In Fig. 4(b), the peaks at 205 and 252 cm^{-1} are assigned to the TO and LO phonon modes of ZnSe NPs with ZB structure, respectively. Similar observations were reported earlier by Shakir et al. [29] No vibration modes, due to impurities, are observed. From previous reports [30–32], the LO phonon frequency of ZnSe NPs was 253 cm^{-1}, and that of single crystal ZnSe was 255 cm^{-1} at room temperature and for ZnSe polycrystalline NPs, the TO and LO phonon frequencies were observed at 210 and 255 cm^{-1}, respectively. In comparison to these results, the LO and TO phonon peaks of the ZnSe NPs are shifted toward lower frequencies, which may be due to the effect of their nano size. The sharp and symmetric Raman peaks of the ZnSe NPs suggest that the synthesized NPs are highly crystalline, in agreement with the results of XRD and TEM. On the basis of the results of Raman and PL, it can be concluded that the ZnSe NPs in the present study possess excellent crystallinity to display sharp and symmetric Raman peaks and a strong NBE emission.

4. Conclusion

In summary, low-toxic ZnSe QDs and NPs were successfully synthesized by an easily controlled method. Effects due to the different structures of the solvent variables were investigated, and the WZ structure was preferred due to the template effect of EN. The obtained ZnSe cubic NPs had good crystallizability and exhibited a strong and stable blue emission peak at 472 nm. While the wurtzite QDs with a diameter of 3–4 nm had a strong main emission band centered at 422 nm. In the Raman spectrum, relative to the bulk crystals of ZnSe, the LO and TO phonon peaks of the ZnSe QDs and NPs both shifted toward lower frequencies, probably due to their small size and high surface area.

Acknowledgments

This work was financially supported by the National Natural Science Foundation of China (Grant No. 61178074, 61008051), the Twentieth Five-Year Program for Science and Technology of Education Department of Jilin Province (Item No. 20110169), Program for the development of Science and Technology of Jilin Province (Item No. 201205078).

References

[1] S. Acharya, D.D. Sarma, N.R. Jana, P. Narayan, J. Phys. Chem. Lett. 1 (2010) 485–488.
[2] L.L. Yang, Q.X. Zhao, M. Willander, X.J. Liu, M. Fahlman, J.H. Yang, Cryst. Growth Des. 10 (2010) 1904–1910.
[3] N. Pradhan, D.M. Battaglia, Y. Liu, X. Peng, Nano Lett. 7 (2007) 312–317.
[4] J. Yang, J. Cao, L. Yang, et al. J. Appl. Phys. 108 (2010), 044304-1-7.
[5] B. Xiang, H.Z. Zhang, G.H. Li, F.H. Yang, F.H. Su, R.M. Wang, J. Xu, G.W. Lu, X.C. Sun, Q. Zhao, D.P. Yu, Appl. Phys. Lett. 82 (2003) 3330–3332.
[6] J. Zhu, Y. Koltypin, A. Gedanken, Chem. Mater. 12 (2000) 73–78.
[7] L. Zhang, H. Yang, J. Yu, F. Shao, L. Li, F. Zhang, H. Zhao, J. Phys. Chem. C 113 (2009) 5434–5443.
[8] C.R. Wang, J. Wang, Q. Li, G.C. Yi, Adv. Funct. Mater. 15 (2005) 1471–1477.
[9] Q. Peng, Y. Dong, Z. Deng, X. Sun, Y. Li, Inorg. Chem. 40 (2001) 3840–3841.
[10] M. Chen, L. Gao, Mater. Chem. Phys. 91 (2005) 437–441.
[11] C.X. Shan, Z. Liu, X.T. Zhang, C.C. Wong, S.K. Hark, Nanotechnology 17 (2006) 5561–5564.
[12] H.S. Chen, B. Lo, J.Y. Hwang, G.Y. Chang, C.M. Chen, S.J. Tasi, S.J.J. Wang, J. Phys. Chem. B 108 (2004) 17119–17123.
[13] K.C. Jason, A.M. Franco, S. Gul, C. Corrado, J.Z. Zhang, Langmuir 27 (2011) 8486–8493.
[14] M.A. Hines, P. Guyot-Sionnest, J. Phys. Chem. B 102 (1998) 3655–3657.
[15] A.B. Panda, S. Acharya, S. Efrima, Y. Golan, Langmuir 23 (2007) 765–770.
[16] A.B. Panda, S. Acharya, S. Efrima, Adv. Mater. 17 (2005) 2471–2474.
[17] S. Acharya, A.B. Panda, S. Efrima, Y. Golan, Adv. Mater. 19 (2007) 1105–1108.
[18] Z.X. Deng, C. Wang, X.M. Sun, Y.D. Li, Inorg. Chem. 41 (2002) 869–873.
[19] N.A. Okereke, I.A. Ezenwa, A.J. Ekpunobi, J. Non-oxide Glasses 3 (2011) 105–111.
[20] Z. Zhu, G.D. Brownlie, P.J. Thompson, K.A. Prior, B.C. Cavenett, Appl. Phys. Lett. 67 (1995) 3762–3764.
[21] Z.D. Hu, X.F. Duan, M. Gao, Q. Chen, L.M. Peng, J. Phys. Chem. C 111 (2007) 2987–2991.
[22] D. Han, C. Song, X. Li, Mater. Chem. Phys. 116 (2009) 41–45.
[23] L. Yang, L. Liu, D. Xiao, J. Zhu, Mater. Lett. 72 (2012) 113–115.
[24] C. Burda, S. Link, M. Mohamed, M. El-Sayed, J. Phys. Chem. B 105 (2001) 12286–12292.
[25] M.I. Vasilevskiy, A.G. Rolo, M.J.M. Gomes, O.V. Vikhrova, C. Ricolleau, J. Phys.: Condens. Matter 13 (2001) 3491–3509.
[26] C. Trallero-Giner, A. Debernardi, M. Cardona, Phys. Rev. B 57 (1998) 4664–4669.
[27] Q. Xiong, J. Wang, O. Reese, L.C. Lew Yan Voon, P.C. Eklund, Nano Lett. 4 (2004) 1991–1996.
[28] X. Fu, H. An, W. Du, Mater. Lett. 59 (2005) 1484–1490.
[29] M. Shakir, S.K. Kushwaha, K.K. Maurya, G. Bhagavannarayana, M.A. Wahab, Solid State Commun. 149 (2009) 2047–2049.
[30] T.J. Mountaiaris, J.D. Peck, S. Stoltz, W.Y. Yu, A. Petrou, P.G. Mattocks, Appl. Phys. Lett. 68 (1996) 2270–2272.
[31] B. Schreder, A. Materny, W. Kiefer, G. Bacher, A. Forchel, G. Landwehr, J. Raman Spectrosc. 31 (2000) 959–963.
[32] D. Sarigannis, J.D. Peck, G. Kioseogiou, A. Petrou, T.J. Mountaiaris, Appl. Phys. Lett. 80 (2002) 4024–4026.